High somato-dendritic coupling of V1 layer 5 neurons independent of behavioural state and visual stimulation

Valerio Francioni[1,2] and Nathalie L. Rochefort[1,2,†]

[1]Centre for Discovery Brain Sciences, School of Biomedical Sciences Edinburgh, Edinburgh, EH8 9XD, United Kingdom.
[2]Simons Initiative for the Developing Brain, University of Edinburgh, Edinburgh, EH8 9XD, United Kingdom.

[†] Corresponding Author:
Nathalie Rochefort
Centre for Discovery Brain Sciences, Biomedical Sciences Edinburgh, Edinburgh, EH8 9XD, United Kingdom.
n.rochefort@ed.ac.uk

Abstract (max 150 words)

Active dendritic conductances impact the integration of synaptic inputs. However, the extent to which dendrites act as independent computational subunits in vivo, remains unclear. We imaged calcium signals in the soma, trunk and distal tuft dendrites of individual layer 5 pyramidal neurons in the primary visual cortex of awake mice, both in darkness and during visual stimulation, while the animal was either running or stationary. We found highly correlated calcium transients in all imaged apical tuft branches and throughout all neuronal compartments (soma, trunk, tuft). However, the frequency of calcium transients was found to decrease in a distance- and amplitude-dependent manner from soma to apical tuft. Visual stimulation and locomotion increased global apical tuft activity but did not alter the coupling between soma and apical tuft. In the apical tuft, branch-specific activity was rare, limited to the smallest calcium transients and independent of visual stimulation and locomotion.

Introduction

Cortical layer 5 excitatory neurons are characterized by long apical dendrites receiving inputs from multiple long-range cortical and subcortical connections (Harris and Shepherd, 2015; Ramaswamy and Markram, 2015). In the primary visual cortex (V1), layer 5 pyramidal neurons display selective responses to physical features of visual stimuli, such as the orientation and direction of movement (Kim *et al.*, 2015). In addition, layer 5 neurons activity is modulated by locomotion both in darkness and during visual stimulation (Erisken *et al.*, 2014; Dipoppa *et al.*, 2016; Dadarlat and Stryker, 2017), suggesting that V1 layer 5 neurons integrate inputs from anatomically and functionally distinct pathways (visual and motor-related). However, the integration of visual and locomotion-related inputs and its relationship with somatic output remains unknown.

Dendritic properties were shown to support both distance-dependent filtering and local dendritic non linearities (Grienberger, Chen and Konnerth, 2015; Stuart and Spruston, 2015). Different types of active dendritic currents have been described to support local nonlinear events, primarily driven by NMDA-receptors Ca and Na- conductances both in vitro

and in vivo (for review, Grienberger, Chen and Konnerth, 2015; Stuart and Spruston, 2015) These dendritic events are generally associated with calcium influx both locally and globally in the apical tuft of layer 5 neurons (Xu *et al.*, 2012; Hill *et al.*, 2013; Palmer *et al.*, 2014; Manita *et al.*, 2015; Takahashi *et al.*, 2016). Additionally, the coincident occurrence of back-propagating action potentials and tuft depolarization was shown to generate widespread calcium transients in the apical tuft dendrites (Lasser-rosst and Lisman, 1992; Spruston *et al.*, 1995; Magee and Johnston, 1997; Helmchen *et al.*, 1999; Larkum, Zhu and Sakmann, 1999; Waters *et al.*, 2003) . The frequency and dynamics of local dendritic nonlinearities in vivo have been a matter of debate, with previous studies giving conflicting results. In the motor cortex, one study suggested that individual branches of densely labelled layer V neurons selectively respond to specific motor outputs and serve as independent computational subunits (Cichon and Gan, 2015). However, other studies suggest that the entire apical tuft acts as a single, independent computational subunit, both in the somatosensory cortex (Xu *et al.*, 2012; Manita *et al.*, 2015; Takahashi *et al.*, 2016) and in the motor cortex (Peters *et al.*, 2017). Events described as dendritically-generated spikes were reported in the visual and somatosensory cortex during sensory stimulation (Smith *et al.*, 2013; Palmer *et al.*, 2014). However, single dendrites recordings prevented conclusions about the branch-specific nature of the detected events. In addition, dendritic spikes displayed similar selectivity as somatic action potentials indicating that these compartments may be strongly coupled with each other (Smith *et al.*, 2013). Other studies reported dendritic spikes in association with backpropagating action potentials during spontaneous activity in the motor cortex (Hill *et al.*, 2013) and sensory stimulation in somatosensory cortex (Svoboda *et al.*, 1997; Kerlin A*et al.* 2018). Differences in recording methods and dendritic signal analysis may explain these discrepancies. So far however, the functional role of local and global dendritic events, including their coupling with somatic output, remains largely unexplored in awake behaving animals.

In this study, we used multiplane, two-photon calcium imaging to semi-simultaneously image different compartments of individual layer V pyramidal neurons in the primary visual cortex (V1) of head-fixed awake behaving mice. We imaged calcium signals in the soma, trunk and distal tuft dendrites, both in darkness and during the presentation of drifting gratings, while the animal was either running or stationary. We found that the vast majority of dendritic calcium transients in the apical tuft were coincident with global events, with rare cases of branch-specific activity, limited to the smallest amplitude events. This global apical tuft activity was found to be highly correlated with somatic activity. Additionally, we found that the frequency of somatic calcium signals was higher than the frequency of apical tuft activity. Indeed, while almost all events observed in the tuft were also visible in the soma, around 40% of somatic events attenuated in an amplitude and distance-dependent manner from the soma to the apical tuft. Finally, our results show that neither visual stimulation nor locomotion affected the coupling between somatic and apical tuft dendritic calcium signals.

Results

Highly correlated, widespread calcium signals in apical tuft dendrites of single L5 neurons

We imaged changes in fluorescence overtime in apical dendrites of single layer 5 pyramidal neurons sparsely labelled with the calcium sensor GCamP6 (Chen *et al.*, 2013) in the primary visual cortex of adult mice. Using two-photon imaging, we monitored changes of GCamP6f signals in individual apical tuft dendrites of head-fixed awake behaving mice that were free to run on a cylindrical treadmill (Figure 1A). Our results showed highly correlated calcium

signals in all apical branches belonging to the same neuron and imaged in a given field of view (Pearson's correlation coefficient ρ =0.92, SEM = 0.01, N = 25 fields of view recorded from 70 branches, 14 neurons, 6 animals) (Figure 1D). Because distal dendrites are thinner, more excitable and more compartmentalised than proximal tuft dendrites, we tested whether the correlation of calcium transients between apical tuft branches decreased with distance from the apical trunk (nexus). We reconstructed each individual neuron for which we imaged the apical tuft and quantified the correlation of fluorescence signals across sibling branches: we found that calcium signals in sibling branches were highly correlated (average Pearson's correlation coefficient ρ = 0.92) regardless of their branching order (One-way ANOVA, p = 0.34) (Figure 1E,F). Using semi-simultaneous imaging of dendrites at different focal planes within the apical tuft of individual layer 5 neurons, we also found highly correlated calcium signals between proximal and distal tuft branches (average Pearson's correlation coefficient ρ=0.88, Figure 2D(i)). Noteworthy, in addition to the global, widespread calcium transients, we also observed in individual spines, independent calcium signals that were not correlated with dendritic signals (supplementary figure 1), indicating that in our experimental conditions, we could resolve independent spine calcium signals.

We then assessed whether this widespread, highly correlated apical tuft activity was modulated by visual stimulation and locomotion. We found that both visual stimulation and locomotion increased mean GCamP6 ΔF/F0 in the apical tuft of layer 5 neurons (average ΔF/F0; repeated measure Two-way ANOVA, p = 0.005, 0.003 and 0.99 for visual stimulation, locomotion and interaction between both conditions, respectively) (Figure 1H). However, the high correlation of calcium signals between all imaged dendritic branches was not significantly different between periods of darkness and visual stimulation (drifting gratings) and between stationary and locomotion periods (Two-way ANOVA, p = 0.43, 0.62 and 0.97 for visual stimulation, locomotion and interaction between both conditions, respectively). Finally, we found that the selectivity of the responses to the drifting gratings orientation, quantified by an orientation selectivity index, also did not affect the high correlation of calcium transients in apical tuft dendrites (Figure S3).

In line with these findings, we found that branch-specific activity in the apical tuft was rare. We quantified the amount of branch-specific activity in all pairs of branches belonging to the same neuron as the proportion of calcium transients present in one branch and absent in the other pair's branch. Among the 70 imaged branches across 14 neurons, branch-specific calcium transients represented less than 3% of the total number of transients. Among all imaged calcium transients, these local signals were dominated by calcium transients of the smallest amplitudes (Figure 1J). In addition, neither visual stimulation with drifting gratings nor locomotion significantly affected this small proportion of branch-specific calcium signals (Three-way ANOVA, p < 10-15for event amplitude and p = 0.29; 0.8 and 0.94, for visual stimulation, locomotion and interaction between both conditions, respectively. No other interaction effect was statistically significant) (Figure 1J). We tested the robustness of our quantification by using different thresholds for the detection of individual calcium transients (supplementary figure 2). We found that varying the threshold did not change our findings: the number of branch-specific events ranged between 0.8 and 3.8% and remained limited to transients of the smallest amplitudes (Figure S2).

Altogether, our results show that apical dendritic calcium signals in V1 layer 5 neurons are almost exclusively dominated by highly correlated calcium transients in the whole apical tuft. Neither visual stimulation nor locomotion modulated this high correlation of apical tuft dendritic calcium signals.

Calcium signals are highly correlated throughout all compartments of individual L5 neurons

We then assessed whether the global, widespread apical tuft calcium signals were coupled with somatic activity. For this, we semi-simultaneously imaged GCamP6s calcium signals at two focal planes, separated on average by 170 µm in depth, in 4 different pairs of neuronal compartments from the soma to the apical tuft: Soma-Trunk, proximal Trunk-distal Trunk, distal Trunk-apical Tuft, proximal Tuft-distal Tuft (Figure 2A,B). We found that calcium transients simultaneously imaged in each pair of proximal and distal compartments were highly correlated (Figure 2C,D). For each pair of compartments, we found that the average Pearson's correlation value between the amplitudes of individual transients was 0.88 between the proximal and distal parts of the apical tuft, 0.92 between the trunk and the apical tuft and 0.85 between the proximal and distal trunk. The lowest correlation value was found between the soma and the proximal trunk (0.74, Figure 2D). For each pair of neuronal compartments, we controlled that shuffling the calcium transients in one compartment resulted in an average correlation value of zero (Figure 2D). Altogether, these results show that calcium transients amplitudes were highly correlated from the soma to the apical tuft of V1 individual layer 5 neurons.

Frequency of calcium transients decreases in a distance- and amplitude dependent manner from soma to apical tuft

We then tested whether the high correlation of calcium transients' amplitudes between soma and apical tuft was associated with distance-dependent changes in the frequency of these events.

We quantified the frequency of calcium events in each pair of proximal and distal compartments imaged semi-simultaneously (Figure 3A). We found that the frequency of calcium transients decreased from proximal to distal compartments (Paired t-test, $p = 1.1e-6$) by an average of 14% from soma to proximal trunk, 8% from proximal to distal trunk, 24% from distal trunk to apical tuft and 22% form proximal tuft to distal tuft. Combined, these proportions indicate a decrease of about 40% of calcium transients from soma to the distal part of the apical tuft (Figure 3B and S4). This result was confirmed by a second data set, in which somatic and apical tuft calcium transients were imaged independently. We found that the mean frequency of calcium transients in the apical tuft corresponded to 62% of the frequency of events in the corresponding soma (supplementary figure 4).

We then checked whether this decrease in frequency depended on the amplitude of the calcium transients. We calculated the percentage of compartment-specific calcium transients as a function of their amplitude (Figure 3C). The vast majority of compartment-specific events were dominated by calcium transients in proximal compartments that were not detected in distal ones (red trace in figure 3C), while only few calcium transients were found in distal compartments and not in the corresponding proximal one (blue trace in Figure 3C) (see also Supplementary video 1 and 2). In addition, our results show that smaller amplitude calcium transients in the proximal compartment were more likely to attenuate below detection level in the distal compartment compared to larger amplitudes events (red trace in figure 3C). As a result, compartment-specific events were dominated by small amplitude calcium transients in proximal compartments (Two-way ANOVA, $p < 10-15$, $p < 10-15$, $p < 10-15$, for compartment (proximal vs distal), amplitude, and interaction effect,

respectively. Figure 4A). We controlled that our results were robust to the threshold we used for detecting calcium transients. When decreasing the threshold for events detection to up to 30% in the distal compartment, we still observed an amplitude-dependent decay of calcium events in the proximal compartment (Figure S2). Similarly, when increasing the threshold by 30% for event detection in the proximal compartment, almost all the events observed distally were also found proximally (Figure S2). Due to the scattering nature of cortical tissue, signal to noise ratio decreased with imaging depth. As a consequence, the distance-dependent decrease in frequency may be underestimated.

These results indicate that at least 40% of somatic calcium transients attenuate in a distance dependent manner along the apical trunk and distal dendrites. Additionally, these findings show that almost all distal events were found in proximal compartments, suggesting two possible mechanisms: either all global apical tuft calcium transients reliably generate somatic action potentials or global tuft activity is triggered by back-propagating action potentials.

Visual stimulation and locomotion do not alter the coupling between soma and apical tuft calcium signals.

We then tested whether visual stimulation and locomotion altered the coupling between the different compartments of individual layer 5 neurons. For each condition, we plotted the percentage of compartment-specific calcium transients as a function of their amplitude and found no significant difference between stationary and locomotion periods and between darkness and visual stimulation (Two-way ANOVA, $p = 0.57$ and $p = 0.14$ for visual stimulation and locomotion, respectively. Figure 4B).

Even though smaller events were attenuated with similar probabilities across the four conditions, calcium transients found in different neuronal compartments, may be amplified or attenuated in a condition-dependent manner (figure 4C). To capture these nonlinearities, we plotted the amplitude of each detected transient in each compartment and calculated a residual value as the distance from the linear robust regression fit. We then plotted the cumulative distribution of the residual value for every calcium transient in all 4 pairs of imaged compartments from soma to apical tuft. We found that, on average, the non-linear changes in calcium transients' amplitude across neuronal compartments were not significantly different between darkness and visual stimulation nor between stationary and locomotion periods (Figure 4D). Finally, our data set included layer 5 pyramidal neurons whose soma was located at different depths within layer 5 from 468 to 666 µm (median 528 µm. Supplementary figure 4). Despite this diversity, we found similar results across the 33 imaged layer 5 neurons with no significant difference in the somato-dendritic coupling of calcium transients across the different conditions.

These results indicate that the coupling between somatic and apical tuft dendritic calcium signals remains unaltered by visual stimulation and locomotion under our experimental conditions.

Discussion

Our results show highly correlated calcium transients in all imaged dendrites of apical tuft and throughout all compartments of individual L5 neurons (soma, trunk, tuft) in the primary visual cortex of awake behaving mice. However, the frequency of calcium transients was found to

decrease in a distance- and amplitude-dependent manner from soma to apical tuft. Whereas almost all transients observed in the tuft were present in proximal compartments, the frequency of calcium transients in apical tuft was about 60% of their frequency in the corresponding soma. This indicates that a substantial fraction (40%) of somatic calcium signals attenuate toward the apical tuft. In the apical tuft, we found that branch-specific calcium transients were rare and limited to small amplitude transients. Neither visual stimulation nor locomotion altered the coupling between soma and apical tuft nor the proportion of branch-specific events.

Limitations of the use of calcium imaging to assess dendritic activity in awake behaving mice

Investigations of local dendritic activity in awake behaving mice have so far mainly relied on the use of genetically-encoded calcium indicators (Xu *et al.*, 2012; Cichon and Gan, 2015; Manita *et al.*, 2015; Takahashi *et al.*, 2016; Sheffield, Adoff and Dombeck, 2017; Kerlin A, Mohar B, Flickinger D, MacLennan B, Davis C, Spruston N, 2018; Ranganathan *et al.*, 2018; Sheffield and Dombeck, 2019). Our results were obtained from imaging fluorescence changes of the calcium indicator GCamP6 in soma and dendrites of individual layer 5 neurons. The analysis of our data set showed that several experimental constraints may mistakenly bias results towards signals interpreted as local dendritic activity. Dense labelling was already demonstrated to strongly affect correlation values (Xu *et al.*, 2012), however, even in cases of relatively sparse labelling of individual neurons, contamination from axons or dendrites of other labelled neurons may lead to local signals detected in single dendrites. In our data set, we systematically reconstructed our imaged neurons and excluded regions of interest where overlapping dendrites from other neurons were observed. Movement artefacts may also lead to inaccurate detection of local dendrite signals; these artefacts are more likely to be found during specific behaviour, such as locomotion, and therefore can bias the interpretation of the results. In our data set we used the activity-independent marker tdTomato to correct for motion artefacts and excluded the recordings in which tdTomato marker was not detected. For most of our imaged neurons, baseline fluorescence of GCamP6 could also be used for the same purpose. Another parameter that may cause artefactual local dendritic signals, is the length of the imaged dendritic segments (and therefore the size of the regions of interest used to extract the changes of fluorescence over time). Small regions of interest could include spines not clearly distinguishable from the corresponding dendritic shaft, especially when the spine is located above the dendrite at the imaged focal plane. As a consequence, in small regions of interests, spine signals may be wrongly interpreted as local dendritic signals.

An additional source of bias is linked to the properties of calcium indicators. Differences in calcium buffering properties of individual compartments lead to different decay times of fluorescent calcium indicators between somatic and dendritic compartments (ref). As a consequence, a longer decay time in one compartment may be detected as an independent event (in a time window in which the corresponding calcium transient in the other compartment would already be back to baseline level). In order to account for this difference, we based our analysis on the detection of peak amplitudes of individual calcium transients. This detection depends on arbitrary thresholds: we thus showed the robustness of our results across different detection thresholds (supplementary figure 2). Finally, our results may be biased by the affinity of GCamP6s: the relationship between GCamP6s and spiking activity was calibrated for layer 2/3 neurons and revealed that this indicator could detect single action potentials (Chen *et al.*, 2013). However, it remains unclear whether this

detection threshold is similar for layer 5 neurons. As a consequence, we cannot exclude that the acquisition of our data, may be biased towards detecting larger events.

Widespread, correlated calcium transients in apical tuft dendritic branches of layer 5 neurons

Our results show that in the apical tuft, branch-specific calcium transients were rare and limited to transients of the smallest amplitudes. These findings suggest that either branch-specific calcium activity is virtually absent and that the entire apical tuft behaves as a single computational unit, or that branch-specific activity is systematically coincident with global tuft calcium events and thus could not be detected in our experimental conditions. Finally, independent local dendritic activity may be underestimated in case these local dendritic events would have an amplitude lower than the detection threshold imposed by the affinity of the calcium indicator and imaging noise. However, our results show clear spine calcium signals and a wide range of calcium transients' amplitudes in dendrites and soma. In addition, in vitro (Golding, Staff and Spruston, 2002; Milojkovic, Zhou and Antic, 2007; Nevian *et al.*, 2007; Antic *et al.*, 2010) and in vivo (Helmchen *et al.*, 1999) experiments performed with calcium indicators have shown that the calcium transients generated by local dendritic spikes were comparable or larger than the transients generated by backpropagating action potentials and were reliably detected in vivo with calcium indicators (Helmchen *et al.*, 1999). This suggests that our experimental conditions would allow the detection of dendritic calcium spikes.

Distance dependent attenuation of calcium signals from soma to apical tuft

Our results show a high coupling between somatic and apical tuft calcium signals. Owing to their slow kinetics, GCamP6 calcium indicators do not provide the temporal resolution to assess in which subcellular compartment calcium events originate. Previous studies have shown that dendritic signals attenuate in a distance-dependent manner, suggesting that at least some of the calcium events generated in one compartment would fully attenuate as they reach the next compartment (Stuart, Schiller and Sakmann, 1997; Helmchen *et al.*, 1999; Vetter, Roth and Häusser, 2001; Larkum *et al.*, 2009). To estimate the lower bound proportion of calcium events generated in the tuft and in the soma, we investigated the proportion of attenuated events in both centrifugal and centripetal directions. Our results show that while around 40% of somatic calcium transients decay by the time they reach the apical tuft, only 1.4% of apical tuft calcium events were not associated with somatic events (Figure 4A). These results indicate that at least 40% of somatic calcium transients were not triggered by apical tuft calcium events, and that these transients attenuated from the soma to the apical tuft. These observations suggest that these calcium transients are associated with back-propagating somatic action potentials. The remaining 60% of somatic calcium signals were highly correlated with global apical tuft calcium signals. This result is consistent with two possible mechanisms: either global apical tuft activation systematically triggers somatic action potentials, or global tuft calcium transients are triggered by back-propagating action potentials alone or in conjunction with tuft synaptic inputs. The occurrence of these different mechanisms cannot directly be tested with calcium indicators due to their low temporal resolution. However, the distance-dependent decrease in the frequency of calcium transients that we found from soma to apical tuft, suggests that at least some of the transients detected in the tuft correspond to calcium signals associated with back-propagating action potentials. Local synaptic inputs in the tuft may then modulate calcium signals triggered by back-

propagating action potentials and facilitate further somatic action potentials firing, consistent with Backpropagation-activated calcium spike (BAC) theory (Larkum *et al.*, 2009; Manita *et al.*, 2015). Alternatively, apical tuft global calcium signals may be generated by tuft synaptic inputs (Xu *et al.*, 2012; Grienberger, Chen and Konnerth, 2015). Local pharmacological applications of sodium channels antagonists in layer V have previously shown that dendritic spike generation is not affected by the blockage of action potential firing (Cichon and Gan, 2015). However, such pharmacological application may also block the activity of dendrite-targeting inhibitory neurons, a condition that may favour the generation of dendritic calcium spikes. Further experiments are needed to resolve these mechanisms.

Finally, several studies have shown that not all dendritic events are associated with detectable calcium signals (Roome, 2018), such as fast Na+ spikes (Helmchen *et al.*, 1999). It is therefore possible that branch-specific computation may be mediated via these currents, and not detected by GCamP6. Previous electrophysiological studies have recorded high frequency Na+ spikes in apical dendrites of V1 layer ⅔ neurons (Smith *et al.*, 2013) and have shown that the frequency of these events, was higher in the dendrites than in the soma (Moore *et al.*, 2017). Future experiments, for example using voltage-sensitive dyes, may provide the temporal resolution to resolve the different types of dendritic events (Chavarha *et al.*, 2018; Adam *et al.*, 2019)

Integration of internal and external inputs in layer 5 neurons in awake behaving mice

The amount and the dynamics of synaptic inputs received by layer 5 pyramidal neurons strongly vary between in vitro and in vivo conditions, between anesthetized and awake animals and between passive sensory stimulation and active learning tasks (Xu *et al.*, 2012; Hong *et al.*, 2018). It is known that in vivo, apical tuft dendrites of layer 5 neurons receive a barrage of thousands of synaptic inputs (Stuart and Spruston, 2015). In awake behaving mice, apical tuft dendrites of V1 layer 5 neurons receive synaptic inputs conveying information about external stimuli (visual stimuli) as well as information about internal variables (arousal/attention, motor activity, predictive signals) (Pakan, Francioni and Rochefort, 2018). Our results show that, in our passive viewing conditions, changes in visual inputs (darkness versus drifting gratings) and locomotion-related inputs do not affect the relationship between somatic and apical tuft calcium signals nor the prevalence of branch-specific dendritic events.

It is however possible that during the active learning of a behavioural task, the synaptic inputs associated with this learning process would lead to different types of dendritic integration than during passive viewing. For example, dendritic integration of multiplicative combinations of sensory and motor inputs in the tuft dendrites of L5 pyramidal neurons has been described during an active sensing task in mouse somatosensory cortex (Ranganathan *et al.*, 2018). In addition, it was proposed that changes in cortical neurons representations during learning would rely on active dendritic signals generating calcium plateau potentials in L5 apical tuft dendrites (Bittner *et al.*, 2015; Grienberger *et al.*, 2017). In that case, somato-dendritic coupling may change during the course of learning (Sheffield, Adoff and Dombeck, 2017). This remains to be tested in the neurons of the visual cortex. Similarly, somato-dendritic coupling may evolve during postnatal development when sensori-motor associations are formed. Recently, it was shown in the mouse primary visual cortex, that dendrites of layer 2/3 neurons increase their coupling during adulthood, as a consequence of decreased responsiveness of dendrite-targeting interneurons to locomotion-related inputs

(Yaeger, Ringach and Trachtenberg, 2019). Further investigations are needed to reveal these mechanisms in layer 5 visual cortical neurons.

Materials and Method

Animals

All experiments and procedures involving animals were approved by the University of Edinburgh Animal Welfare and the ethical review board (AWERB) and performed under the appropriate PIL and PPL license from the UK Home Office in accordance with the Animal (Scientific Procedures) act 1986 and the European Directive 86/609/EEC on the protection of animals used for experimental purposes.

Adult males and females aged between 8 and 10 weeks obtained from Jackson Laboratory, ME, USA (B6.Cg-Gt(ROSA)26Sor$^{tm14(CAG-tdTomato)Hze}$/J [RRID:IMSR_JAX:007914]) were used for experiments. Animals were group caged in groups of 2-6 animals, with a running wheel on a reverse 12:12 hour light: dark cycle. They were allowed ad libitum access to food and water.

Surgical procedures

Viral delivery of GCaMP6

To obtain sparse labelling of excitatory neurons we used a cre-dependent approach. AAV1.CamKII.GCaMP6f.WPRE.hGH (Penn Vector core, catalogue No. V4673MI-R) was diluted 1:10000 – 1:20000 while either AAV1.Syn.Flex.GCaMP6f.WPRE.SV40 (Penn Vector Core, catalogue No. CS0215) or AAV1.Syn.Flex.GCaMP6s.WPRE.SV40 (Penn Vector Core, catalogue No. CS0408) were diluted 1:10 in the final solution. All dilutions were made in ACSF sterilized using a 0.2 µm syringe filter. AAV1.Syn.Flex.GCaMP6f.WPRE.SV40 was used for experiments in the apical tuft, while AAV1.Syn.Flex.GCaMP6s.WPRE.SV40 was used for semi-simultaneous two-planes imaging.

Animals were anaesthetized by inhalation of 4% Isoflurane and maintained anaesthetised using 1-2% isoflurane. The animal's body temperature was maintained at physiological levels using a closed-loop, adjustable heating pad monitoring the animal's temperature via a rectal probe. Eye cream (Bepanthen, Bayer) was applied to protect the eyes from dryness and light exposure.

After induction of anaesthesia, mice were shaved, mounted onto a stereotaxic frame (David Kopf instruments, CA, USA) and head-fixed using ear bars. An analgesic was administered subcutaneously (Vetergesic, buprenorphine, 0.1 mg/kg of body weight). Layer V was targeted stereotactically. Injections were performed on the left hemisphere of the brain using a glass pipette (20 µm tip diameter. Nanoject, Drummond Scientific), backfilled with the viral preparation, using a nanoject II (Drummond Scientific), at 2 different depths, 650 and 500 µm from brain surface. A total volume of 73.6 nl was injected across the two sites (8x 4.6 nl at each location). Single 4.6 nl injections were spaced 30s from one another to allow sufficient time for diffusion. After each injection, pipettes were left in situ for an additional 5 min to prevent backflow. The scalp was then sutured (Ethicon, Ethilon polyamide size 6) and the animal monitored during recovery in a heated cage before returning to its home cage for 2-3 weeks.

Headplate and imaging window

Under anaesthesia (isoflurane), mice were shaved, mounted onto a stereotaxic frame (David Kopf instruments, CA, USA) and head-fixed using ear bars. Analgesic and anti-inflammatory drugs were administered subcutaneously (Vetergesic, buprenorphine, 0.1 mg/kg of body weight; Carpaphen, Carprieve, 5mg/kg of body weight; Dexamethasone, Rapidexon, 2mg/kg of body weight). For a cranial window over V1, a section of scalp was removed, the underlying bone was cleansed before a rectangular craniotomy of ~ 2x1.5 mm was made over the left primary visual cortex. The dura was kept intact. The craniotomy was then sealed with a glass cover slip and fixed with cyanoacrylate glue. To stabilize the brain during imaging, we used a triple glass window by stacking three cover-slip glasses (Menzel-Glaser 24x32 mm # 0) on top of each other. These were glued together using an optically clear UV-cured glue (Norland Optical adhesive). Overall, the thickness of the glass window inserted through the cranial window, was comparable to the thickness of the skull at the time of imaging (Smith *et al.*, 2017).

A custom-built metal headplate was fixed on top of the skull with glue and cemented with dental acrylic (Paladur, Heraeus Kulzer). At the end of the procedure, a single dose of 25ml/kg of Ringer's solution was injected subcutaneously to rehydrate the animal after the procedure. The animal was then released from the head fixation and returned to a heated recovery cage, until full motor capacity was recovered.

In vivo two-photon imaging data acquisition

Imaging was performed using a 25x Objective (Olympus). The excitation wavelength of the laser was set to 920 nm. Layer V pyramidal neurons were recorded between 500 and 650 µm below the brain surface and followed up to their distal tuft dendrites along the apical trunk. Neurons which had their nucleus filled with GCaMP6 or had blobby-looking dendrites were excluded for recording. At the end of each imaging session, a z-stack was acquired to allow a more detailed, offline morphological reconstruction of the imaged neuron. Reconstructions were done using the ImageJ plugin Simple Neurite Tracer. Imaging was performed using a 570 nm short-pass dichroic mirror and two single-band pass filters, a 525/50 (Scientifica) for GCaMP6 light absorption, and a 620/60 (Scientifica) for TdTomato absorption.

Habituation and imaging started 2–3 weeks after AAV injection. Mice were habituated to head-fixation in the dark for 45 min and began to run freely on a polystyrene cylinder (20 cm diameter, on a ball-bearing mounted axis). The mice's running speed on the circular treadmill was continuously monitored using an optical encoder (E7P, 250cpr, Pewatron, Switzerland) connected to a data acquisition device (National Instrument, UK) with custom-written software in LabView (National Instrument, UK) and analysed in MATLAB (Mathworks, MA)

Single-plane two-photon imaging data were acquired using a custom-built galvo-resonant scanning system with a Ti:Sapphire pulsing laser (Chameleon Vision-S, Coherent, CA, USA; < 70 fs pulse width, 80 MHz repetition rate) at 120 Hz, with a custom-programmed LabVIEW-based software (version 8.2; National Instruments, UK). Multi-plane data were acquired using an ultra-fast, solid-state, single 100 fs pulse width laser (InSight DeepSee, SpectraPhysiscs, CA, USA) and a FemtoSmart Dual two-photon microscope (Femtonics, Budapest, Hungary). Two focal planes, average distance of 170 µm on the vertical plane at a frequency of 4-7Hz for each plane were acquired semi-simultaneously using a Piezo objective positioner kit (P725.4CA, Physic Instruments, Germany).

Visual stimulation

Visual stimuli were generated using the Psychophysics Toolbox package (Brainard, 1997) for MATLAB (Mathworks, MA) and displayed on a custom-modified backlit LED monitor (51 × 29 cm, Dell, UK) placed 20 cm from the right eye, covering 104° × 72° of the visual field. Visual stimulation trials consisted of drifting full-field square-wave gratings for 3 seconds (spatial frequency of 0.05 cycles per degree, 1.5 Hz, 8 equally spaced directions in randomized order, contrast 80%, mean luminance 37 cd/m^2). Drifting gratings were separated from one another by 4 seconds of isoluminant grey periods. Time stamps for the onset of every stimulus were recorded and aligned to imaging frames using custom-built Matlab scripts.

Data Analysis

Image analysis and signal extraction

To correct for brain motion after image acquisition, we used 2D plane translation-based image alignment (SIMA 1.2.0, sequential image analysis; Kaifosh et al., 2014). We 3D reconstructed each imaged neuron and defined regions of interest (ROIs) corresponding to neuronal cell body and dendritic segments manually. Due to sparse labelling, signal contamination was negligible in most cases. In cases ROIs were contaminated by labelled structures from other neurons, we excluded those ROIs from further analysis.

The pixel intensity within each ROI was averaged to create a raw fluorescence time series F(t). Baseline fluorescence F0 was computed for each neuron by taking the fifth percentile of the smoothed F(t) (1 Hz lowpass, zero-phase, 60th-order FIR filter) over each trial (F0(t)), averaged across all trials. As a consequence, the same baseline F0 was used for computing the changes in fluorescence in darkness and during visual stimulation. The change in fluorescence relative to baseline, ΔF/F0 was computed by taking the difference between F and F0(t) and dividing by F0.

Single plane data was acquired at 120 Hz, and subsequently downsampled to 5Hz for signal processing. Multi-plane data were acquired and analysed at 4-7 Hz.

Calcium transients analysis

We used the built-in Matlab function findpeaks to detect individual calcium transients, using a threshold of 2.8 std above noise. We tested the robustness of our results to different thresholds +/- 30% of the selected threshold (see Supplementary figure 2). For each peak found in any branch or compartment, we defined an event as coincident in another branch or compartment when it occurred in a time window of 3 seconds around the frame where the first peak was originally detected (2 seconds before, 1 after). 99% of coincident events were observed within +/- 0.73 ms. Each event could only be considered coincident with one peak. The amplitude of a calcium event was determined by taking the difference between the ΔF/F0 amplitude at the frame in which a peak was detected and a local minimum in a 2 seconds, backward sliding window. Correlation values were calculated as the Pearson's correlation values between event amplitudes in pairs of branches or compartments. Shuffling values were obtained by randomly shuffling the order of the events in one branch or compartment of each pair analysed. Residuals were extracted by calculating the robust linear regression line between normalised event amplitudes in two compartments, and then extracting the distance, along the y-axis, of each individual point from this robust line.

Locomotion analysis

Changes in the position of the cylindrical treadmill (sampled at 12,000 Hz) were interpolated to match the rate of imaging. To define stationary and locomotion periods we used the following criteria: Stationary corresponded to periods where the instantaneous speed (as measured at the 40 Hz sampling rate) was less than 0.1 cm/s. Locomotion corresponded to periods meeting three criteria: instantaneous speed ≥ 0.1 cm/s, 0.25 Hz lowpass filtered speed ≥ 0.1 cm/s, and an average speed ≥ 0.1 cm/s over a 2 s window cantered at this point in time. Any inter-locomotion interval shorter than 500 ms was also labelled as locomotion. Stationary periods less than 3 s after or 0.2 s before a period of locomotion were removed from the analysis.

Orientation Selectivity

The orientation selectivity index (OSI) was calculated as $(O_{pref}-O_{orth})/(O_{pref}-O_{orth})$ where O_{pref} represents the mean ΔF/F0 value during the presentation of the preferred orientation across trials and O_{orth} represents the mean ΔF/F0 value at the orthogonal orientation compared to preferred. The preferred stimulus of each neuron was the orientation that elicited the maximal response when averaged across all trials.

Statistics

All analysis was performed either in Matlab 2017a, or in GraphPad Prism 8. All error bars in the figures represent standard error of the mean. The details of the statistical test we used, as well the details about what we used as independent samples can be found in the relevant figure legends.

Acknowledgments

We thank the GENIE Program and the Janelia Research Campus, specifically V. Jayaraman, R. Kerr, D. Kim, L. Looger, and K. Svoboda, for making GCaMP6 available. This work was funded by the Wellcome Trust and the Royal Society (Sir Henry Dale fellowship to N.R.), the Marie Curie Actions of the European Union's FP7 program (MC-CIG 631770 to N.R.), the Shirley Foundation, the Patrick Wild Center and the RS MacDonald Charitable Trust Seedcorn Grant (to N.R.), the Simons Initiative for the Developing Brain (to N.R.) and the University of Edinburgh (PhD scholarship to V.F.).

Declaration of Interests

The authors declare no competing interests

References

Adam, Y. *et al.* (2019) 'Voltage imaging and optogenetics reveal behaviour-dependent changes in hippocampal dynamics', *Nature*. Springer US. doi:

10.1038/s41586-019-1166-7.

Antic, S. D. *et al.* (2010) 'Review The Decade of the Dendritic NMDA Spike', 3001(June), pp. 2991–3001. doi: 10.1002/jnr.22444.

Bittner, K. C. *et al.* (2015) 'Conjunctive input processing drives feature selectivity in hippocampal CA1 neurons', 18(8). doi: 10.1038/nn.4062.

Chavarha, M. *et al.* (2018) 'Fast two-photon volumetric imaging of an improved voltage indicator reveals electrical activity in deeply located neurons in the awake brain', *BioRXiv*.

Chen, T.-W. *et al.* (2013) 'Ultrasensitive fluorescent proteins for imaging neuronal activity.', *Nature*, 499(7458), pp. 295–300. doi: 10.1038/nature12354.

Cichon, J. and Gan, W.-B. (2015) 'Branch-specific dendritic Ca 2 1 spikes cause persistent synaptic plasticity', *Nature*. doi: 10.1038/nature14251.

Dadarlat, X. M. C. and Stryker, X. M. P. (2017) 'Locomotion Enhances Neural Encoding of Visual Stimuli in Mouse V1', 37(14), pp. 3764–3775. doi: 10.1523/JNEUROSCI.2728-16.2017.

Dipoppa, M. *et al.* (2016) 'Vision and locomotion shape the interactions between neuron types in mouse visual cortex'.

Erisken, S. *et al.* (2014) 'Effects of Locomotion Extend throughout the Mouse Early Visual System', *Current Biology*. Elsevier Ltd, 24(24), pp. 1–9. doi: 10.1016/j.cub.2014.10.045.

Golding, N. L., Staff, N. P. and Spruston, N. (2002) 'Dendritic spikes as a mechanism for cooperative long-term potentiation', 418(July). doi: 10.1038/nature00836.1.

Grienberger, C. *et al.* (2017) 'Inhibitory suppression of heterogeneously tuned excitation enhances spatial coding in CA1 place cells', 20(3). doi: 10.1038/nn.4486.

Grienberger, C., Chen, X. and Konnerth, A. (2015) 'Dendritic function in vivo', *Trends in Neurosciences*. Elsevier Ltd, 38(1), pp. 45–54. doi: 10.1016/j.tins.2014.11.002.

Harris, K. D. and Shepherd, G. M. G. (2015) 'The neocortical circuit: themes and variations', *Nature Neuroscience*, 18(2), pp. 170–181. doi: 10.1038/nn.3917.

Helmchen, F. *et al.* (1999) 'In vivo dendritic calcium dynamics in deep-layer cortical pyramidal neurons'.

Hill, D. N. *et al.* (2013) 'Multibranch activity in basal and tuft dendrites during fi ring of layer 5 cortical neurons in vivo', 2013. doi: 10.1073/pnas.1312599110/-/DCSupplemental.www.pnas.org/cgi/doi/10.1073/pnas.1312599110.

Hong, Y. K. *et al.* (2018) 'Letter', *Nature*. Springer US. doi: 10.1038/s41586-018-0527-y.

Kerlin A, Mohar B, Flickinger D, MacLennan B, Davis C, Spruston N, S. K. (2018) 'Functional clustering of dendritic activity during decision-making Keywords', *BioRXiv*.

Kim, E. J. *et al.* (2015) 'Three Types of Cortical Layer 5 Neurons That Differ in Brain-wide Connectivity and Function', *Neuron*. Elsevier Inc., 88(6), pp. 1–15. doi: 10.1016/j.neuron.2015.11.002.

Larkum, M. E. *et al.* (2009) 'Synaptic Integration in Tuft Dendrites', 663(August), pp. 756–761.

Larkum, M. E., Zhu, J. J. and Sakmann, B. (1999) 'A new cellular mechanism for coupling inputs arriving at different cortical layers', 398(March), pp. 2–5.

Lasser-rosst, N. and Lisman, J. E. (1992) 'hippocampal neurons', 357(May), pp. 244–246.

Magee, J. C. and Johnston, D. (1997) 'A Synaptically Controlled , Associative Signal for Hebbian Plasticity in Hippocampal Neurons', 275(January), pp. 209–214.

Manita, S. *et al.* (2015) 'A Top-Down Cortical Circuit for Accurate Sensory Perception', *Neuron*. Elsevier Inc., 86(5), pp. 1304–1316. doi: 10.1016/j.neuron.2015.05.006.

Milojkovic, B. A., Zhou, W. and Antic, S. D. (2007) 'Voltage and calcium transients in basal dendrites of the rat prefrontal cortex', 2, pp. 447–468. doi: 10.1113/jphysiol.2007.142315.

Moore, J. J. *et al.* (2017) 'freely behaving rats', *Science*. doi: 10.1126/science.aaj1497.

Nevian, T. *et al.* (2007) 'Properties of basal dendrites of layer 5 pyramidal neurons : a direct patch-clamp recording study', 10(2), pp. 206–214. doi: 10.1038/nn1826.

Pakan, J. M., Francioni, V. and Rochefort, N. L. (2018) 'Action and learning shape the activity of neuronal circuits in the visual cortex', *Current Opinion in Neurobiology*. The Authors, 52, pp. 88–97. doi: 10.1016/j.conb.2018.04.020.

Palmer, L. M. *et al.* (2014) 'NMDA spikes enhance action potential generation during sensory input', *Nature Publishing Group*. Nature Publishing Group, 17(3), pp. 383–390. doi: 10.1038/nn.3646.

Peters, A. J. *et al.* (2017) 'Reorganization of corticospinal output during motor learning', 20(8). doi: 10.1038/nn.4596.

Ramaswamy, S. and Markram, H. (2015) 'Anatomy and physiology of the thick-tufted layer 5 pyramidal neuron', *Frontiers in Cellular Neuroscience*, 9(June), pp. 1–29. doi: 10.3389/fncel.2015.00233.

Ranganathan, G. N. *et al.* (2018) 'Active dendritic integration and mixed neocortical network representations during an adaptive sensing behavior', *Nature Neuroscience*. Springer US. doi: 10.1038/s41593-018-0254-6.

Roome, C. J. (2018) 'neurons in awake mice', *Nature Communications*. Springer US, (2018), pp. 1–14. doi: 10.1038/s41467-018-05900-3.

Sheffield, M. E. and Dombeck, D. A. (2019) 'Dendritic mechanisms of hippocampal place field formation', *Current Opinion in Neurobiology*. Elsevier Ltd, 54, pp. 1–11. doi: 10.1016/j.conb.2018.07.004.

Sheffield, M. E. J., Adoff, M. D. and Dombeck, D. A. (2017) 'Increased Prevalence of Calcium Transients across the Dendritic Arbor during Place Field Formation', *Neuron*. Elsevier Inc., 96(2), pp. 490-504.e5. doi: 10.1016/j.neuron.2017.09.029.

Smith, I. T. *et al.* (2017) 'Stream-dependent development of higher visual cortical areas', *Nature Neuroscience*, 20(2), pp. 200–208. doi: 10.1038/nn.4469.

Smith, S. L. *et al.* (2013) 'Dendritic spikes enhance stimulus selectivity in cortical neurons in vivo.', *Nature*, 503(7474), pp. 115–20. doi: 10.1038/nature12600.

Spruston, N. *et al.* (1995) 'Activity-Dependent Action Potential Invasion and Calcium Influx into Hippocampal CA1 Dendrites', 268(April).

Stuart, G. J. and Spruston, N. (2015) 'Dendritic integration: 60 years of progress', *Nature Neuroscience*, 18(12), pp. 1713–1721. doi: 10.1038/nn.4157.

Stuart, G., Schiller, J. and Sakmann, B. (1997) 'Action potential initiation and propagation in rat neocortical pyramidal neurons', pp. 617–632.

Svoboda, K. *et al.* (1997) 'In vivo dendritic calcium dynamics in neocortical pyramidal neurons.', *Nature*, 385(6612), pp. 161–165. doi: 10.1038/385161a0.

Takahashi, N. *et al.* (2016) 'modulate perception', 354(6319).

Vetter, P., Roth, a and Häusser, M. (2001) 'Propagation of action potentials in dendrites depends on dendritic morphology.', *Journal of neurophysiology*, 85(2), pp. 926–937. doi: 10.1073/pnas.1301224110.

Waters, J. *et al.* (2003) 'Supralinear Ca 2 ƨ Influx into Dendritic Tufts of Layer 2 / 3 Neocortical Pyramidal Neurons In Vitro and In Vivo', 23(24), pp. 8558–8567.

Xu, N. *et al.* (2012) 'Nonlinear dendritic integration of sensory and motor input during an active sensing task.', *Nature*. Nature Publishing Group, 492(7428), pp. 247–51. doi: 10.1038/nature11601.

Yaeger, C. E., Ringach, D. L. and Trachtenberg, J. T. (2019) 'Letter', *Nature*. Springer US, 56. doi: 10.1038/s41586-019-0963-3.

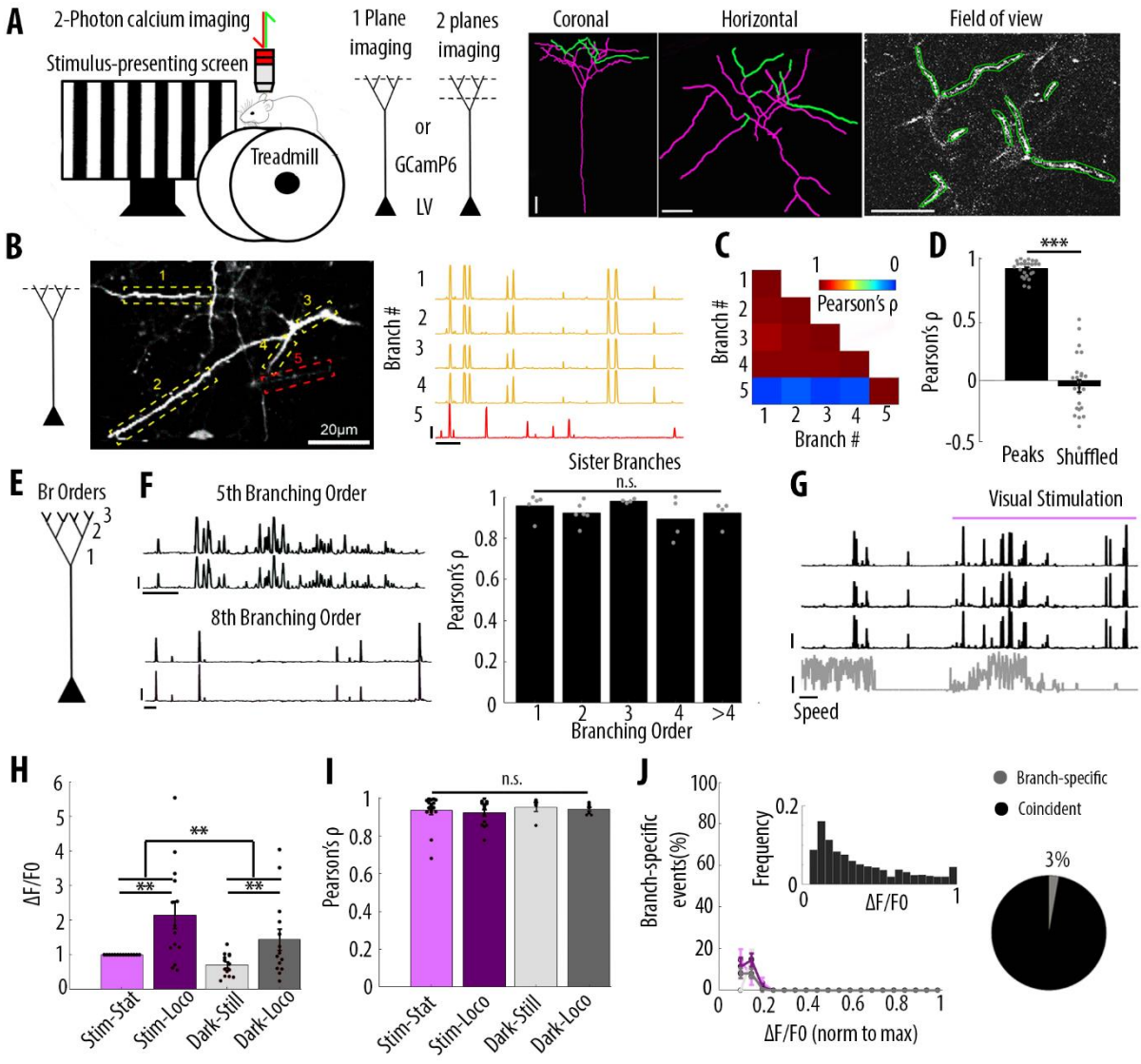

Figure 1. Highly correlated activity in the whole apical tuft of layer V pyramidal neurons
A) Schematic of the methodological approach. Calcium transients were recorded either in multiple apical tuft dendrites in a single focal plane, or semi-simultaneously in different compartments of the neuron (Soma, Trunk and Tuft). At the end of each imaging session, a z-stack was recorded for post-hoc reconstruction of each imaged neuron. B) Single plane imaging of the apical tuft branches of an individual layer V neuron. Calcium transients of the apical tuft branches belonging to one neuron are shown in yellow and calcium transients of tuft branch belonging to a different neuron is shown in red. Scale bars, 0.3ΔF/F0 (normalised to max), 20 s. C) Pearson's correlation matrix between the calcium activity of the branches shown in B. Branches that belong to the same neuron (neuron 1) have a mean Pearson's correlation of 0.96, while the branch that belongs to the different neuron (neuron 2) has a mean Pearson's correlation value of 0.13 with neuron 1's branches. D) Mean Pearson's correlation value ρ for each imaged field of view (FoV) and corresponding shuffled data (Paired t-test, p = 3.5e-15; mean = 0.92 and -0.04; SEM = 0.01 and 0.05; N = 25 FoV; 14 neurons; 6 animals; 70 branches). E) Schematic of our definition of branching orders. F) Two representative traces of sibling branches belonging to the 5th and 8th (left panel, labelled) branching order and a quantification of the Pearson's correlation ρ for sibling tuft branches of different branching orders (right

panel). (For 1st, 2nd, 3rd, 4th and more than 4th branching order, One-way ANOVA, p = 0.34; mean = 0.96; 0.92; 0.98; 0.89; 0.92; N = 5; 6; 4; 4; 4 pairs of branches, respectively). Scale bars, 0.3 ΔF/F0 (normalised to max), 20 s. G) Representative traces of 3 tuft branches belonging to the same neuron while the animal was either stationary or locomoting (lower panel) during either darkness or the presentation of drifting grating (purple segment). Scale bars, 12 cm/s, 0.3ΔF/F0 (normalised to max), 20 s. H) Mean ΔF/F0 for apical tuft dendrites during darkness and visual stimulation while the animal was either stationary of locomoting. Bar graph is normalised to visual stimulation during still condition. Both visual stimulation and locomotion significantly increase the mean ΔF/F0 of tuft branches without any interaction effect (Repeated Measures Two-way ANOVA on log-transformed data, p = 0.0053, 0.0026 and 0.99 for the visual stimulation, locomotion and interaction effects respectively. mean = 0.7; 0.84; 0.37; 0.68; SEM = 0.34; 0.24; 0.12; 0.24; N= 14 neurons). I) Pearson's correlation coefficients ρ for the apical tuft branches of individual neurons during the four conditions (stim and still, stim and loco, dark and still, dark and loco). (Two-way ANOVA, p = 0.43, 0.62 and 0.97 for visual stimulation, locomotion and interaction effects. mean = 0.93; 0.92; 0.95 and 0.94. SEM = 0.02; 0.02; 0.02 and 0.01. N =16; 14; 5 and 7 FoVs respectively. Only FoVs in which at least 6 calcium transients were detectable were included in the calculation of Pearson's ρ). J) Weighted mean of the proportion of branch-specific events as a function of event's amplitude for the four different conditions (lower left panel). Neither visual stimulation nor locomotion nor an interaction effect, increased the number of branch specific events (Three-way ANOVA, p = 0.29; 0.8 and 0.94, respectively. p < 10-15 for event amplitude). Upper left panel, distribution of the events detected in the apical tuft branches. Right panel, pie chart showing that on average 3% of the total events were detected in only one branch.

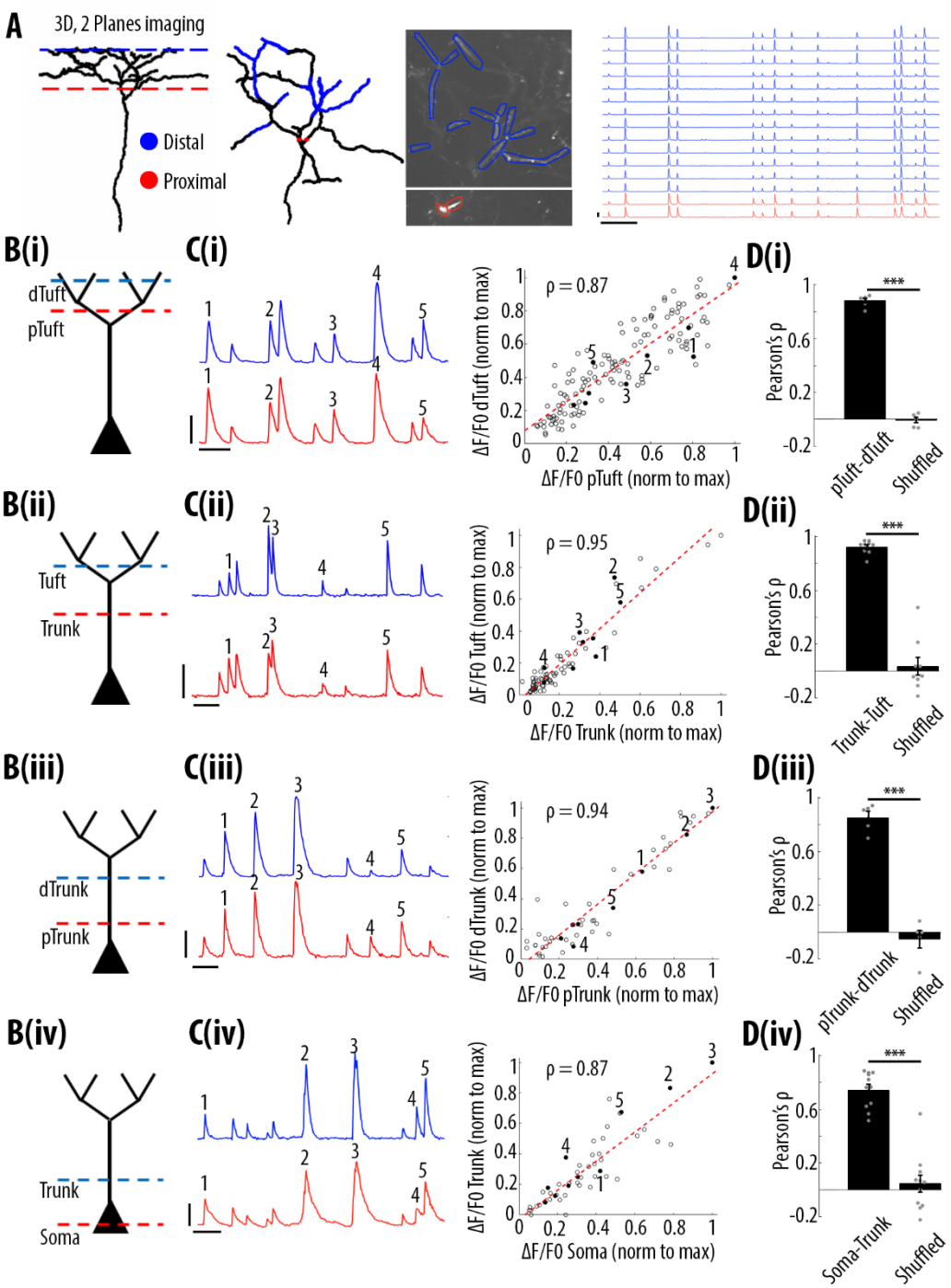

Figure 2. High correlation of calcium transients from soma to apical tuft dendrites of individual layer V neurons

A) Schemata showing the morphological reconstruction of a neuron imaged at two focal planes semi-simultaneously. Left panel, coronal view of the imaged neuron. Red and blue dotted lines indicate the planes of imaging. Middle left panel, horizontal view of the same neuron. Branches highlighted in red and blue, represent the same dendritic branches observed in the middle right panel. Right panel, each trace represents the calcium activity of an individual branch shown in the middle panels. B) Schemata of the compartments imaged simultaneously. C) Left panel, representative calcium events recorded in two neuronal compartments semi-simultaneously as shown in B. Right panel, scatter plot showing the correlation of the amplitude of calcium transients in each compartment simultaneously imaged, and shown in B. Each dot represents a calcium transient. Filled dots are the same transients shown in the left panel and indicated by

numbers. Scale bars 0.3ΔF/F0 (normalised to max), 10 s. D) Pearson's correlation values ρ for each pair of compartments imaged semi-simultaneously and compared to its corresponding shuffled data (Paired t-test, (iv) Soma-Trunk, p = 4.4e-6 mean ρ = 0.74 and 0.05, SEM = 0.04 and 0.06, respectively. N = 11. pTrunk-dTrunk(iii), p = 4.4e-4, mean ρ = 0.85 and -0.05, SEM = 0.05 and 0.07, respectively. N = 5. Trunk-Tuft(ii), p = 8e-7 mean ρ = 0.92 and 0.04, SEM = 0.02 and 0.07, respectively. N = 9. pTuft-dTuft(i), p = 1.6e-6 mean ρ = 0.88 and 0.01, SEM = 0.02 and 0.02, respectively. N = 6).

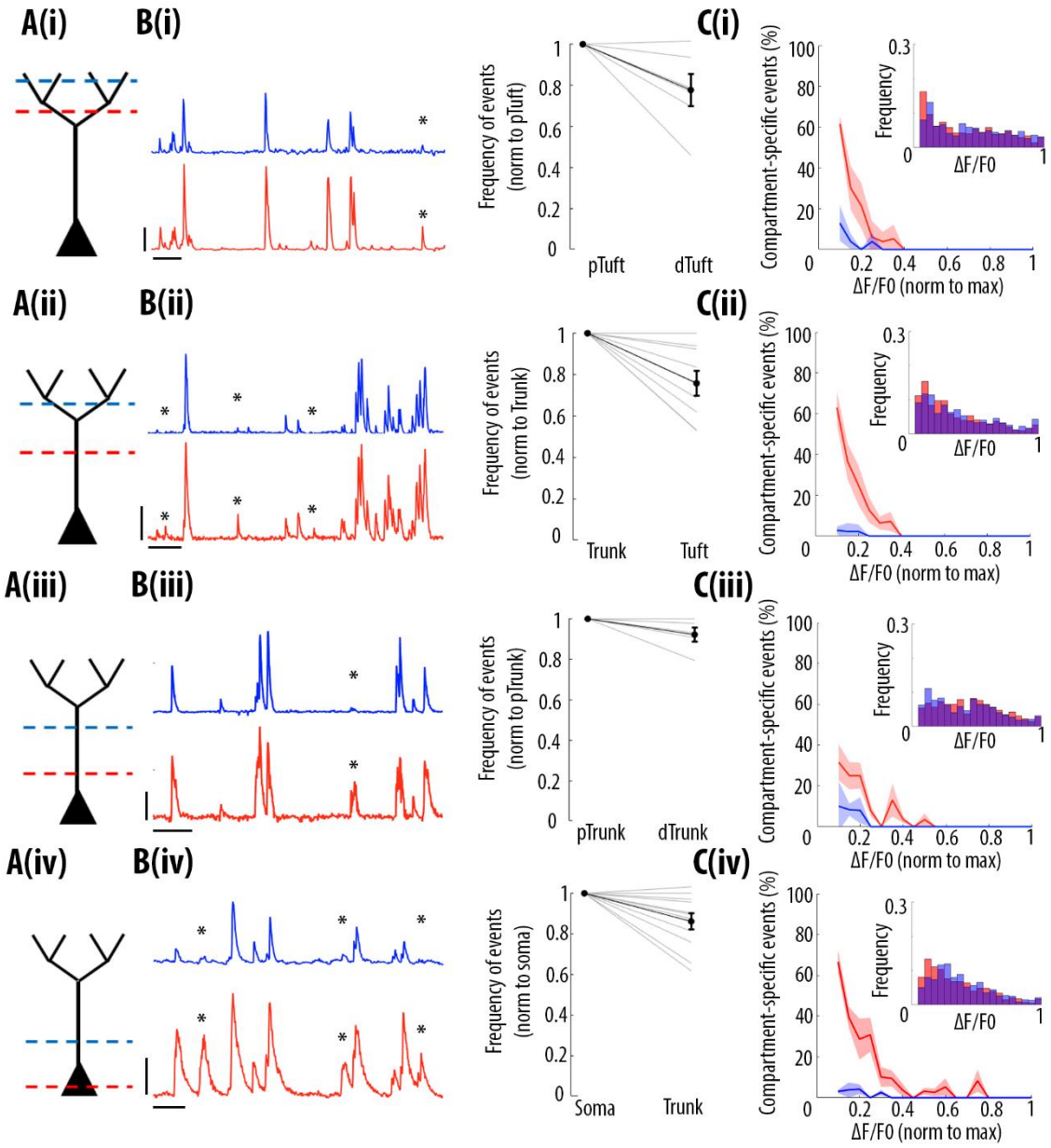

Figure 3. Frequency of calcium transients decreases in a distance and amplitude-dependent dependent manner from the soma to the apical tuft

A) Schemata of the compartments imaged simultaneously. B) Left panel, representative ΔF/F0 traces of calcium activity recorded semi-simultaneously in two different compartments of individual neurons. Asterisks indicate calcium transients detected in the proximal compartment and not detected in the distal one. On the right panel, the frequency of detected calcium transients, normalised to the proximal compartment. Individual lines represent individual neurons (Paired t-test Soma-Trunk(iv), p = 0.007, mean = 0.86, SEM = 0.04, respectively. N =

11 neurons. pTrunk-dTrunk(iii), p = 0.094, mean = 0.92, SEM = 0.03, respectively. N = 5 neurons. Trunk-Tuft(ii), p = 0.003, mean = 0.76, SEM = 0.06, respectively. N = 9 neurons. pTuft-dTuft(i), p = 0.037, mean = 0.78, SEM = 0.08. N = 6 neurons. Altogether, Proximal-Distal direction = p = 1.1e-6, mean = 0.82, SEM = 0.03, N = 29 pairs of compartments from 19 neurons). Scale bars 0.25 ΔF/F0 (normalised to max), 20 s. C) Proportion of compartment-specific events as a function of calcium transients' amplitude. In red, proportion of events detected in the proximal compartment only. In blue, proportion of events detected in the distal compartment only. Upper right panel, in red and blue the frequency histogram of calcium transients amplitudes detected in the proximal and distal compartments, respectively. Thick line represent the weighted mean proportion. Shaded area represents the weighted SEM for each bin (0.05 size). For all compartments, event amplitude, compartment (proximal vs distal) and an interaction between these two factors significantly affected the proportion of compartment-specific events (Two-way ANOVA, Soma-Trunk(iv), $p < 10\text{-}15$, $p < 10\text{-}15$ and $p < 10\text{-}15$, respectively. N = 11 neurons. pTrunk-dTrunk(iii), $p = 1.3\text{x}10\text{-}13$, $p = 2.4\text{x}10\text{-}4$, $p = 7\text{x}10\text{-}3$, respectively. N = 5 neurons. Trunk-Tuft(ii), $p < 10\text{-}15$, $p = 3.4\text{x}10\text{-}9$, $p < 10\text{-}15$, respectively. N = 9 neurons. pTuft-dTuft(i), $p < 10\text{-}15$, $p = 7.8\text{x}10\text{-}5$, $p = 6.2\text{x}10\text{-}8$, respectively. N = 6 neurons. Altogether, Proximal-Distal direction $p < 10\text{-}15$, $p < 10\text{-}15$, $p < 10\text{-}15$, respectively. N = 29 compartments from 19 neurons. See also Figure 4A).

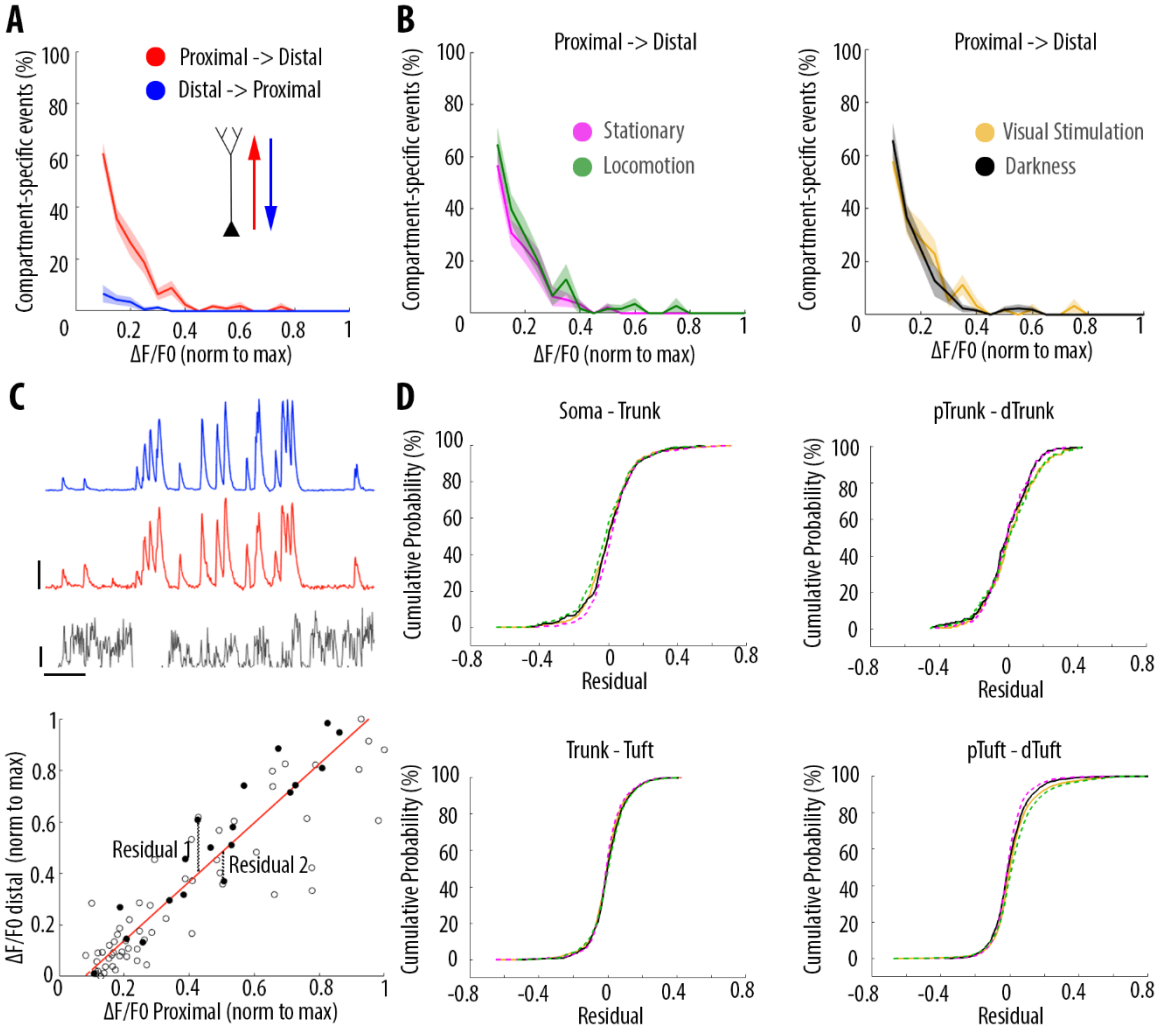

Figure 4. Locomotion and visual stimulation do not alter the relationship between somatic and dendritic activity in individual layer V pyramidal neurons

A) Mean proportion of compartment-specific events as a function of calcium transient amplitude. Data points from figure 3C(i-iv) have been averaged together. In red, events found in the proximal, but not in the distal compartment. In blue, events that are found in the distal, but not proximal compartment. Event amplitude, compartment (proximal vs distal) and an interaction between these two factors significantly affected the proportion of compartment-specific events (Two-way ANOVA, $p < 10\text{-}15$, $p < 10\text{-}15$, $p < 10\text{-}15$. N = 29 pairs of compartments from 19 neurons). B) Neither visual stimulation nor locomotion alter the curve describing amplitude-dependent decay of events in the proximal-to-distal direction (Two-way ANOVA, $p = 0.57$ and $p = 0.14$ for visual stimulation and locomotion, respectively). C) Upper panel, representative trace of the proximal and distal compartment imaged semi-simultaneously during visual stimulation and darkness, during stationary and locomotion periods. Lower panel, scatter plot between the amplitudes of calcium transients for the ΔF/F0 trace shown above. Individual dots represent individual calcium transients. Filled dots are the same as shown in the upper panel. The red line represents the robust linear regression fit. For

each transient, a residual from the robust linear regression was calculated. Scale bars represent 0.25 ΔF/F0 (normalised to max), 20 s. D) Cumulative distribution function for the residuals calculated for each pairs of compartments and for each condition. Neither visual stimulation nor locomotion alter the relationship between somatic and dendritic activity in individual layer V neurons (Paired t-test for the effect of visual stimulation and locomotion on residuals: Soma-Trunk(iv), p = 0.33 and 0.30, respectively. N = 11 neurons. pTrunk-dTrunk(iii), p = 0.34 and 0.93, respectively. N = 5 neurons. Trunk-Tuft(ii), p = 0.5 and 0.95, respectively. N = 9 neurons. pTuft-dTuft(iv), p = 0.83 and 0.08, respectively. N = 6 neurons. Altogether p = 0.62 and 0.96 respectively, N = 29 pairs of compartments from 19 neurons).

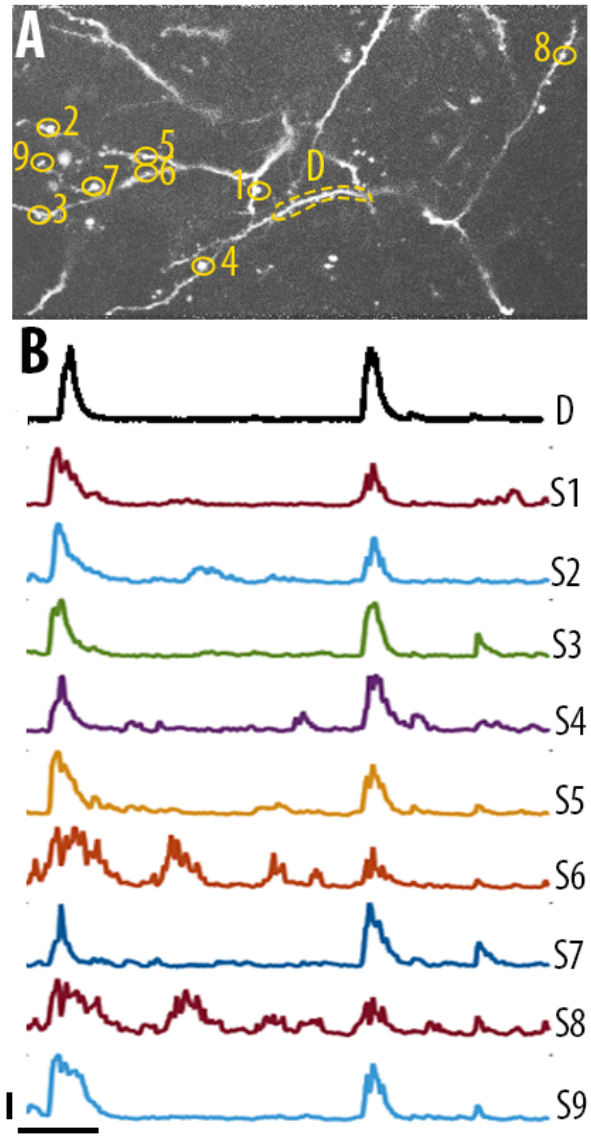

Figure S1. Independent single spine activity in the apical tuft dendrites of layer 5 neurons A) Field of view showing the apical tuft branches of an individual GCamP6-labelled layer V neuron. B) ΔF/F0 traces for individual spines during a single, 65 seconds-long trial. Error bars indicate 0.3ΔF/F0, 10 s.

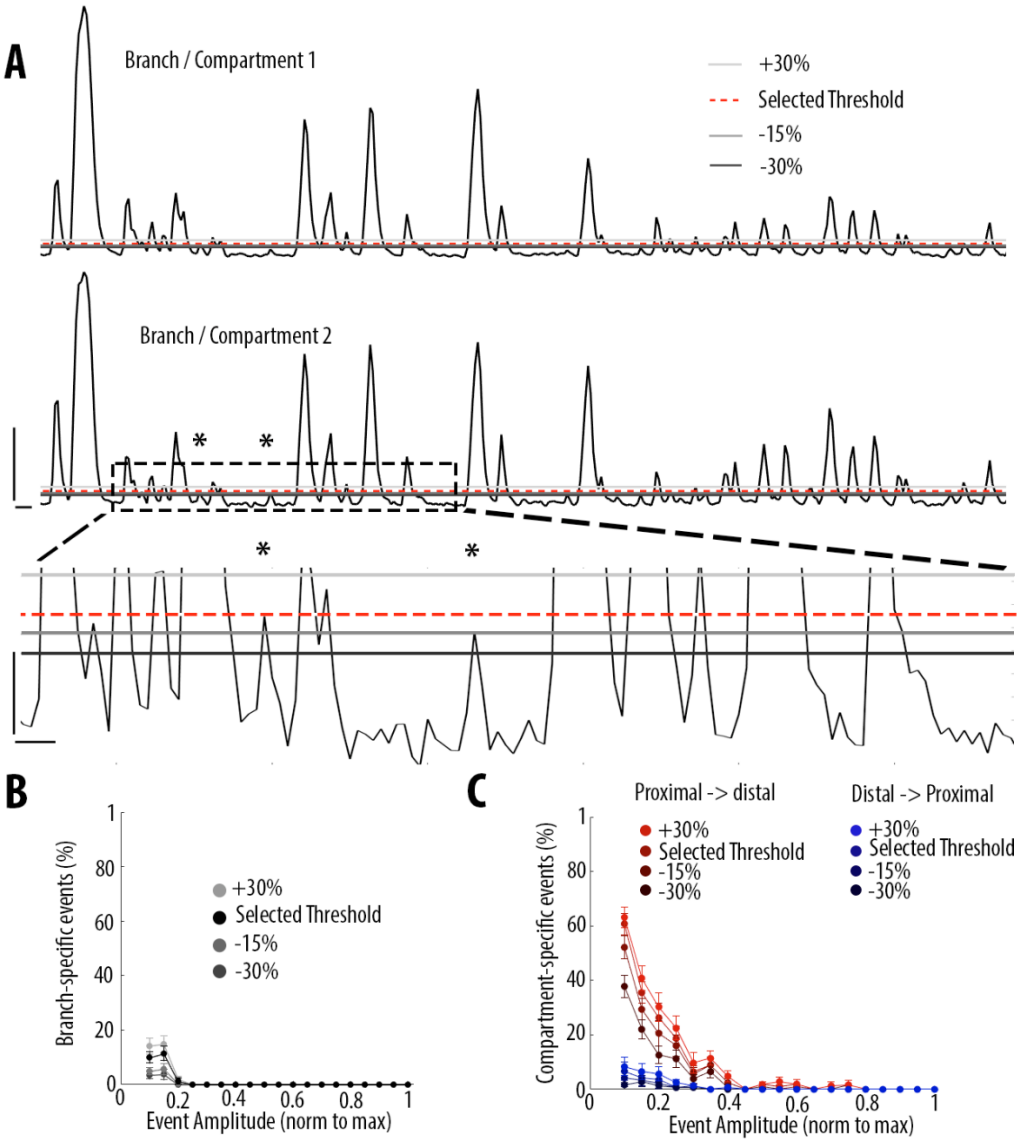

Figure S2. Exploration of parameters space by increasing and decreasing the threshold for calcium transients detection

A) To assess the amount of branch / compartment specific events, for every transient present in one branch / compartment, we assessed whether there was another a corresponding event in the second branch / compartment.

Upper part, ΔF/F0 traces of two sibling branches in the apical tuft branches of a single layer V pyramidal neurons. Asterisks indicate two events which were not detected using the selected threshold but were then detected lowering the threshold by 30%. Lower panel, zoomed image of the dotted area in the upper panel. To assess the resilience of our observed effects to different thresholds, we assessed the amount of branch / compartment specific events, keeping the selected threshold in one branch / compartment (red-dotted line) and varying the threshold in the second branch / compartment from +30% to -30% (light, medium and dark grey lines, respectively). Scale bars: 0.3 ΔF/F0 (normalised to max), 5 s (upper panel); 0.03 ΔF/F0, 1s (lower panel). B) The number of branch-specific events varies as a function of the amplitude and threshold selected. C) The number of compartment-specific events varies as a function of the amplitude and threshold selected.

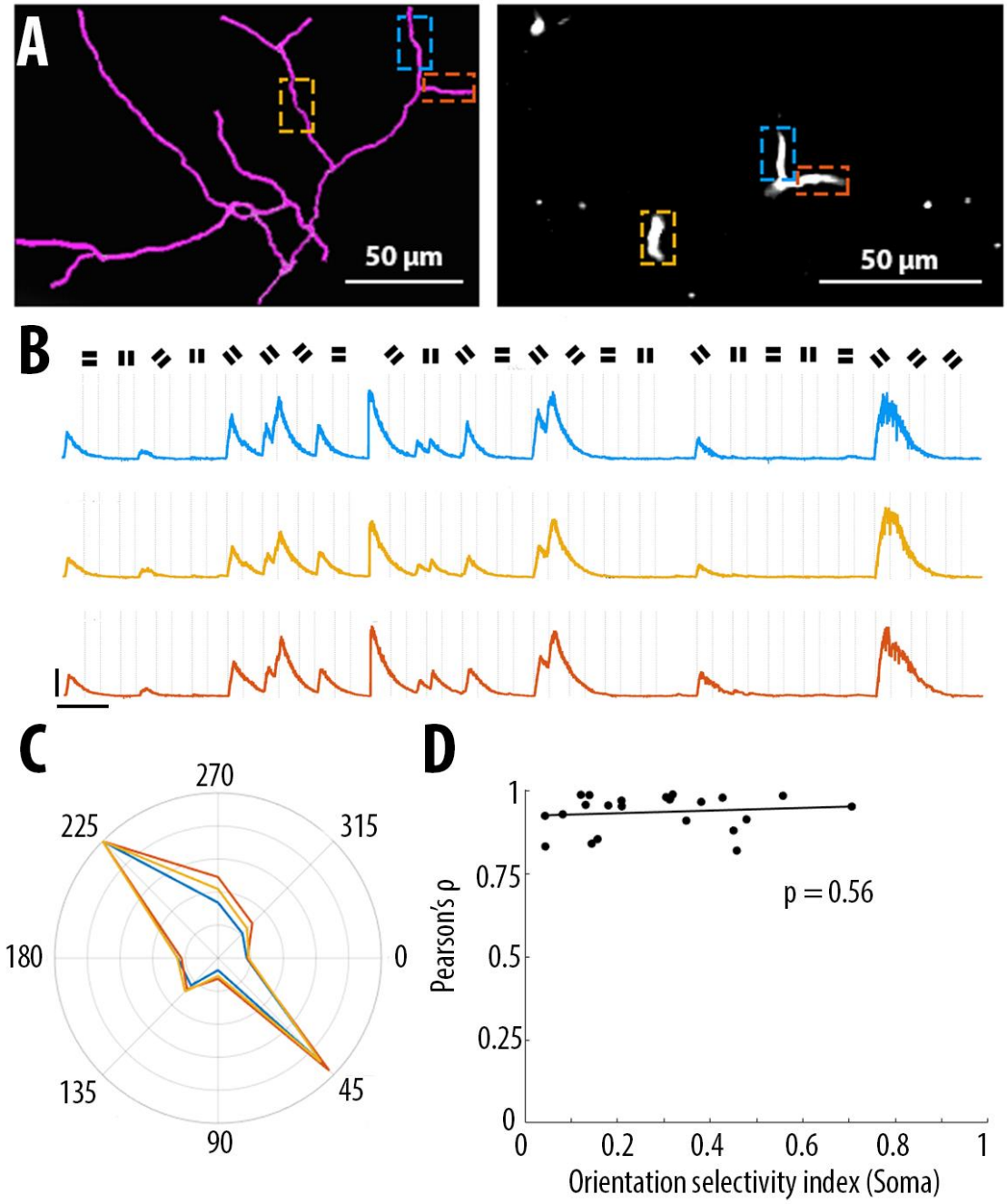

Figure S3. High correlation of calcium transients in apical tuft dendrites, independent of somatic orientation selectivity.

A) The morphological reconstruction of the imaged of three apical tuft branches that were imaged during the presentation of drifting gratings. B) ΔF/F0 traces of the branches shown in A, in response to drifting gratings of different orientations. The space in between two gratings was spaced by an isoluminant grey screen. Scale bars 0.3 ΔF/F0 (normalised to max), 10 s. C) Polar plot quantifying the responses of these 3 branches to different angled stimuli. D) A quantification of the mean Pearson's correlation value ρ, as a function of Orientation Selectivity. The upper panel shows the OSI in the soma, as a function of the mean correlation value of its branches. The lower panel shows the mean OSI for the apical tuft branches in each field of view, as a function of their mean Pearson's correlation value ρ. The straight black line

represents the best fit. In the figure the is reported the p value for the correlation between Pearsons's ρ and OSI.

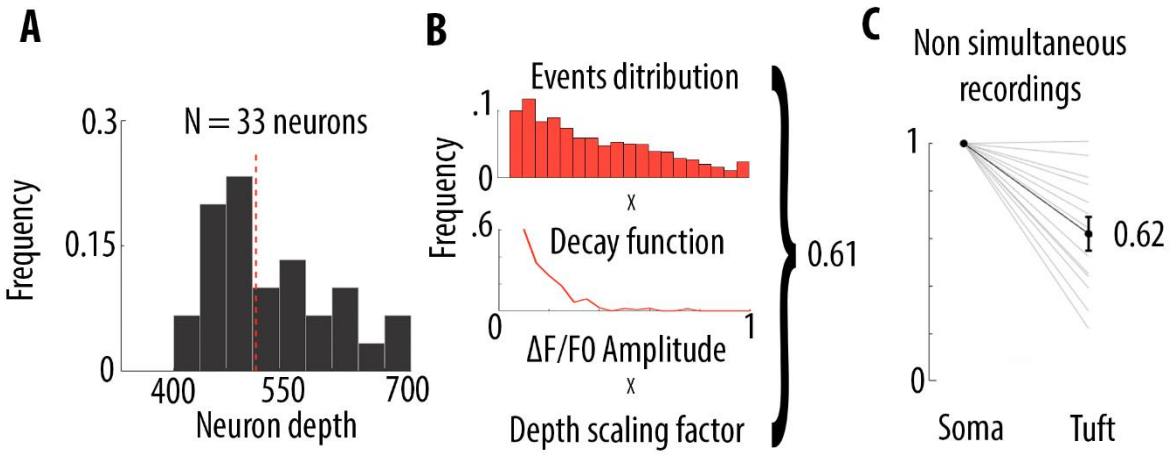

Figure S4. Decreased frequency of calcium events from soma to apical tuft
A) The frequency distribution of the depths at which neurons have been imaged. The red dotted line indicates the median (528 μm from dura). B) An extrapolation of the proportion of the proportion of somatic events, decayed in the tuft. Using the event distribution for all the calcium events (mean of proximal distributions from figure 3), and applying the amplitude-dependent decay function, extrapolated at a distance of 170 μm and projected to the median soma depth we recorded, we calculated the proportion of events that decay from the soma to the tuft (39%). C) Proportion of events in the tuft, compared to the soma when we record these two compartments non-simultaneously.